Heliyon

ELSEVIER

*Received:*
20 July 2015
*Revised:*
11 October 2015
*Accepted:*
16 November 2015

Heliyon (2015) e00050

# Degradable polyethylene nanocomposites with silica, silicate and thermally reduced graphene using oxo-degradable pro-oxidant

**Fakhruddin Patwary, Vikas Mittal** *

*Department of Chemical Engineering, The Petroleum Institute, Abu Dhabi, UAE*

* Corresponding author. Tel.:+ 0097126075491.

E-mail address: vmittal@pi.ac.ae (V. Mittal).

## Abstract

Polyethylene nanocomposites with silica, alumino-silicate and thermally reduced graphene were generated by adding pro-oxidant additive. Additive resulted in early degradation of pure polymer, however, the degradation was delayed in the presence of fillers. Graphene resulted in maximum extent of enhancement of peak degradation temperature (13–14 °C depending on the additive content) followed by silicate and silica. Additive also resulted in enhancement of polymer crystallinity, which was further aided by the filler, though no change in peak melting and crystallization temperatures was observed. The graphene and silicate particles were also observed to be uniformly dispersed in polymer matrix, whereas some aggregates were present in silica based composites. In graphene composite with 2.5 wt% additive content, the tensile modulus was increased by 1.95 times that of pure polymer. Increasing the additive content was also observed to enhance the mechanical performance. For instance, graphene nanocomposite with 1 % additive content had 40 % and 33 % increment in storage modulus at 50 °C and 70 °C respectively as compared to pure PE. The thick plaques of composites exhibited oxo-degradation in the presence of pro-oxidant with silica and silicate composites with 2.5 wt% additive having 100 % degree of embrittlement in 15–16 months at 30 °C.

http://dx.doi.org/10.1016/j.heliyon.2015.e00050

Graphene composites also exhibited ~50 % embrittlement for the same conditions. The filler particles were observed to delay the time needed to attain embrittlement due to reduction in oxygen permeation in the matrix as well as UV absorption, however, these materials confirmed that degradation of the materials could be successfully tuned without sacrificing the mechanical, thermal and rheological properties of the nanocomposites.

Keywords: Engineering, Chemical engineering, Nanotechnology, Materials science

## 1. Introduction

To reduce polymer waste and environmental pollution, the use of degradable polymers has been often stressed, and it is further beneficial, if the degradation can be tuned in accordance with needed service life [1,2]. High molecular weight and hydrophobicity of the commercial polyolefins hinder their direct biodegradation by microbes. It is thus evident that the polymer molecular weight has to be reduced in order to facilitate microbial attack on the chains leading to bio-digestion [3, 4]. During oxo-biodegradation process, UV light, heat and catalytic metals help in oxidative chain scission with the help of atmospheric oxygen, followed by biodegradation phase [2]. Albertsson et al. mentioned that the initial abiotic oxidation step is very important and it is the rate-determining step for the whole degradation process [3]. Temperature and/or sunlight lead to abiotic oxidation and yield low molecular weight polymer fragments for biotic degradation. In case of high density polyethylene (PE), though the polymer does not contain any functional groups in its molecular structure that can absorb UV radiation, it still undergoes partial photo-degradation due to UV absorption by residual catalysts, thermal processing degradation products, process impurities and fillers (if any) present in it [5]. Photo-oxidation has also been reported to be enhanced by incorporating photoinitiators such as chromophores into the materials or by copolymerization with a small amount of monomers that contain carbonyl groups, or by using transition metal compounds such as metal stearate and dithiocarbamates [6]. Some literature studies have analyzed the photo-oxidation (or oxo-degradation) of PE in the presence of pro-oxidants based on metal ions [7, 8, 9]. Chain cleavage occurring by the catalytic action of pro-oxidants has been reported to induce oxidation. The oxidized PE with lower molecular weight and higher hydrophilicity is thus more susceptible to microbial attack. PE blends with biodegradable polymers have also been incorporated with pro-oxidants to accelerate oxidation and to enhance biodegradation [8].

Aerobic biodegradation of the product of thermo-oxidative degradation of polyethylene films containing pro-oxidant under controlled composting conditions was analyzed by Jakubowicz [10]. Mn-stearate was the pro-oxidant


http://dx.doi.org/10.1016/j.heliyon.2015.e00050

and the samples were 30 μm thick. The degree of bio-assimilation after 180 days of incubation was 57.9 to 62 % depending on the amount of pro-oxidant present in the samples. Biodegradability of UV-irradiated films of ethylene-propylene copolymer, isotactic polypropylene (PP) and low density polyethylene was also studied in composting conditions [11]. Weight loss analysis showed that copolymer having lower percentage of ethylene degraded faster. These findings thus confirmed the advantage of oxo-biodegradation approach in achieving controlled degradation of polyolefin films.

Polymer nanocomposites are the organic-inorganic hybrid materials, in which at least one dimension of the filler phase is less than 100 nm [12, 13, 14, 15, 16, 17, 18, 19, 20]. These materials lead to enhancement of mechanical and thermal properties of the polymers due to achievement of nanoscale dispersion of filler particles in the polymer matrix [12, 13, 14, 15, 16, 17, 18, 19, 20]. It is also of importance to study the degradation behavior of the polymer nanocomposites in conjunction with the other physical properties in order to establish their environmental friendliness. Some recent studies have analyzed the effect of different inorganic fillers on the oxo-degradation of PE [21, 22]. Tidjani and Wilkie [21] reported an increase in photo-oxidation of polypropylene in the presence of organically modified clay. Qin et al. [22] also reported that the rate of photo-oxidative degradation of PE nanocomposite generated by incorporating organically modified silicate was much faster than pure PE. The authors attributed this effect to the ammonium ion based surface modification on the surface of clay platelets. On the other hand, addition of zinc oxide was also reported to decrease the rate of photo-degradation of PE as compared to pure polymer [23]. Kumanayaka [24] also reported PE nanocomposites with clay modified with pro-oxidant. The photo-degradation was faster than pure polymer and composite without pro-oxidant till 5 % filler content, after which increasing amount of filler did not affect the photo-oxidation behavior.

In the current study, the effect of amount of metal ion based pro-oxidant and different fillers on the mechanical and thermal performance as well as photo-degradation of thick PE moldings was investigated. Fillers included 0-D and 2-D synthetic nanomaterials like silica, alumino-silicate (without surface modification) and thermally reduced graphene. The composites were generated by melt blending and the weathering properties were studied in conjunction with mechanical, thermal, rheological and morphological properties.

## 2. Materials and methods

### 2.1. Materials

Oxo-biodegradable PE based masterbatch Reverte BD92771 was donated by Wells Plastics, UK. The masterbatch contained a proprietary metal ion based


http://dx.doi.org/10.1016/j.heliyon.2015.e00050

pro-oxidant developed for 1 % addition in thin PE films to achieve shelf life of 9 months at 30 °C [25]. Synthetic silicon dioxide powder (ZEOFREE® 5161 S) and synthetic alumino-silicate (ZEOLEX® 23) were supplied by J. M. Huber Private Limited, India. Thermally reduced graphene was produced by thermal exfoliation of precursor graphite oxide using modified Hummer's method as reported earlier [26, 27]. Matrix polymer i.e. high density polyethylene BB2581 was received from Abu Dhabi Polymers Company Limited (Borouge), UAE and was used as obtained. The polymer was in the form of white pellets with a specific gravity of 0.958 and melt flow index of 0.35 (190 °C/ 2.16 kg, g/10 min).

## 2.2. Materials processing

Melt mixing using mini twin conical screw extruder (MiniLab HAAKE Rheomex CTW5, Germany) was carried out to generate PE-additive blends and PE nanocomposites. Oxo-degradation agent was mixed at two levels of 1 wt% and 2.5 wt%, whereas the filler content was fixed at 5 wt% in the nanocomposites. The compounding temperature was 170 °C at 80 rpm screw speed and 10 min processing time. All the materials were physically premixed in a small bowel before feeding into the extruder. Tetrahedron MTP-10 hot press was used to compression mold the extruded samples. A temperature of 170 °C was used along with a pressure of 270 bars applied for 1 min. The samples were cooled down to 50 °C at a rate of 5 °C/min and a holding pressure of 90 bars was maintained. Sheets of 12*12 cm with a thickness of 1.5 mm were produced for generating disc, dumbbell and bar-shaped test specimens.

## 2.3. Characterization of nanocomposites

Netzsch thermogravimetric analyzer (TGA) was used to analyze the thermal degradation properties of the samples. Nitrogen was used as a carrier gas and the scans were obtained from 50 to 700 °C at a heating rate of 10 °C/min. The samples were dried for 48 h under vacuum before testing. LINSEIS STA PT1600 TGA system was also used to measure the weight change during heating in air atmosphere. This system is coupled with a Phipher mass spectrometer (MS) which allowed to determine the elimination of $H_2O$ (m/z = 18), $CO_2$ (m/z = 44) and other fractions during heating. All measurements were performed using a heating rate of 3 °C/min, using flow rate of 20 ml/min.

Netzsch differential scanning calorimetric (DSC) was used to obtain the calorimetric analysis of the polymer blends and nanocomposites under nitrogen atmosphere. The scans were obtained from 30-250-30 °C using heating and cooling rate of 5 °C/min.


http://dx.doi.org/10.1016/j.heliyon.2015.e00050

Rheological properties were characterized using AR 2000 rheometer from TA Instruments. Disc shaped samples of 25 mm diameter and 2 mm thickness were characterized at 170 °C using a gap opening of 1 mm. Frequency sweep scans (dynamic testing) of the materials were recorded at 1 % strain from $\omega = 0.01$ to 600 rad.s$^{-1}$. Dynamic mechanical analyzer (DMA) RSA3 of TA Instruments was used to study the change in modulus with temperature (25–100 °C). Dynamic temperature ramp test was used at a frequency of 5 rad.s$^{-1}$ on bar-shaped samples, using a ramp rate of 3 °C/min and 1 % strain for all nanocomposites. Tensile properties were analyzed on the universal testing machine Testometric M-350 10CT. The dumbbell-shaped samples of 53 mm length, 4 mm width and 2 mm thickness conforming to standard ASTM-638-V were used. A loading rate of 10 mm/min was used and the tests were carried out at room temperature. An average of six values is reported.

Transmission electron microscopy (TEM) analysis of the nanocomposite samples was performed in bright field using Philips CM 20 (Philips/FEI, Eindhoven) electron microscope at 120 kV and 200 kV accelerating voltages. Thin sections of 70–90 nm thickness were microtomed from the sample block and were supported on 100 mesh grids sputter coated with a 3 nm thick carbon layer. For morphology characterization of the materials using wide angle X-ray diffraction, Panalytical Powder Diffractometer (X'Pert PRO) using CuKα radiation ($\lambda = 1.5406$ A°) in reflection mode was used. Zero-background holder was used to minimize the noise. The samples were step-scanned from 10–70° 2θ at room temperature using a step size of 0.02° 2θ and a step time of 10 s.

The samples were subjected to testing of their oxo-degradation properties in Wells Plastics' laboratory at Stone, Staffordshire, UK. Thick plaques with dimensions 19 × 9 × 1.4 mm were aged using modified ASTM D5208-01 (Cycle C) test method. The ageing cabinet contained UV lamps to simulate gentle outdoor sunlight (irradiance 0.89 ± 0.02 W/(m$^2$.nm)). The temperature of the cabinet was maintained at 50 °C. The test pieces were subjected to UV light up to 12 weeks in the cabinet, thus, the actual UV exposure was relatively slight and the acceleration of the ageing process was due to the higher temperature (50 °C) following the photo-triggering stage of the breakdown reaction. The test specimens were removed after fixed time periods and the carbonyl index was determined by infra-red analysis, using modified ASTM D5576test method to suit the analysis of polyolefins incorporated with additives. The carbonyl index at the point at which each test piece was fully embrittled was noted and presented as 100 % embrittlement. The remaining carbonyl indices were calculated as a percentage of this and reported as “degree of embrittlement”. Finally, Arrhenius principles were applied to the results obtained at 50 °C, transposing them into the real-time results that would be expected at 30 °C.


http://dx.doi.org/10.1016/j.heliyon.2015.e00050

## 3. Results and discussion

Fig. 1a demonstrates the TGA thermograms of the PE-additive blends and PE nanocomposites in comparison with pure PE and additive. Table 1 also shows the peak degradation temperatures as well as mass loss between 300–400 °C and 400–460 °C. The PE polymer used in the additive had lower thermal stability than the matrix PE used in the study and exhibited multiple degradation plateaus. The residual weight after degradation to 800 °C was 4 %, which indicated the weight fraction of metal ions present in the additive. The addition of 1 % additive to PE did not affect its peak degradation temperature, however, the enhanced additive content of 2.5 % reduced the thermal performance as observed from slight decrease in peak degradation of PE from 477 to 474 °C. The mass loss between 300–400 °C and 400–460 °C was also observed to increase as a function of additive content indicating accelerated degradation of polymer in the presence of additive. The fillers were observed to provide varying degrees of high temperature stabilization as evident from delayed peak degradation temperature in the nanocomposites. The mass loss in the composites as compared to PE-additive blends was also reduced, but was generally higher than pure PE due to combined effect of filler and additive. Similar to PE, increasing the amount of additive in the composites resulted in slight reduction in thermal stability. Graphene composites were most stable as the composites exhibited an increment of 13–14 °C in the peak degradation temperature and the weight loss at higher temperature was even less than pure PE. Fig. 1b further quantifies the thermal stability by reporting the time taken by the materials to have 1 % and 5 % loss of mass during the TGA analysis. As compared to 18 and 23 min for pure PE to lose 1 % and 5 % mass, the PE + 2.5 % additive blend exhibited the loss at 11 and 15 min respectively. In contrast, graphene composites with 2.5 % additive content had 1 % and 5 % mass loss at 28 and

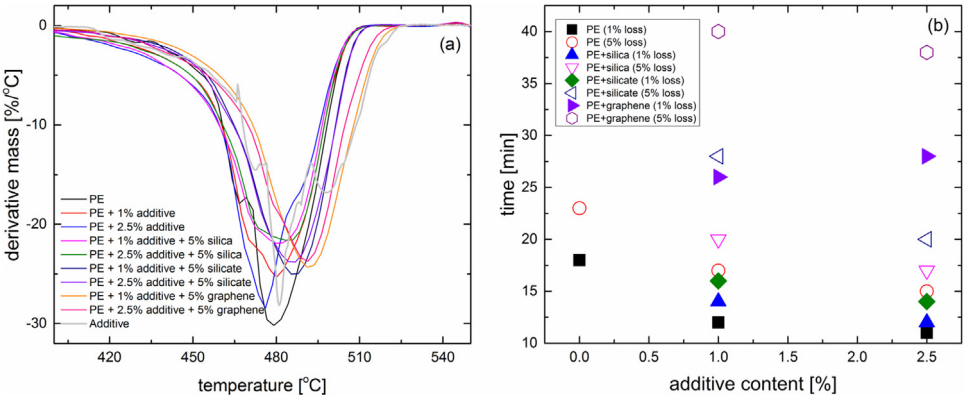


**Fig. 1.** (a) TGA differential thermograms of additive, PE, PE-additive blends and PE nanocomposites; (b) time taken to degrade 1 % and 5 % of these samples plotted as a function of additive content.


http://dx.doi.org/10.1016/j.heliyon.2015.e00050

**Table 1.** Peak degradation temperature and mass loss between 300–400 °C and 400–460 °C for PE, PE-additive blends and PE nanocomposites.

| Polymer/Nanocomposite | Peak degradation temperature [°C] | Mass loss between 300–400 °C [%] | Mass loss between 400–460 °C [%] |
|---|---|---|---|
| Pure PE | 477 | 1.0 | 12.5 |
| PE + 1 % additive | 477 | 2.4 | 19.8 |
| PE + 2.5 % additive | 474 | 2.7 | 22.4 |
| PE + 1 % additive + 5 % silica | 480 | 1.9 | 19.4 |
| PE + 2.5 % additive + 5 % silica | 480 | 2.5 | 20.5 |
| PE + 1 % additive + 5 % silicate | 485 | 2.4 | 12.5 |
| PE + 2.5 % additive + 5 % silicate | 484 | 2.5 | 14.8 |
| PE + 1 % additive + 5 % graphene | 491 | 1.8 | 10.2 |
| PE + 2.5 % additive + 5 % graphene | 490 | 2.3 | 12.2 |

38 min indicating significant thermal stabilization provided by the graphene platelets. The slowing down of rate of degradation on the addition of additive and fillers contradicted the results from Lee et al. [28] due to the octadecylamine swelling agent used in their study. In addition, the compatibilizers used in their study are also occasionally observed to induce reduction in thermal and mechanical performance of the matrix polymer due to their low molecular weight [29]. The degradation of PE-additive and PE composites with 2.5 % additive content was also studied through TGA-MS in air atmosphere. As shown in Fig. 2, the additive though did not alter the degradation mechanism of PE, but caused faster degradation. The evolution of degradation products with m/z = 18 ($H_2O$) and m/z = 44 ($CO_2$) was observed at lower temperatures in the blend as compared to pure PE. The composite with

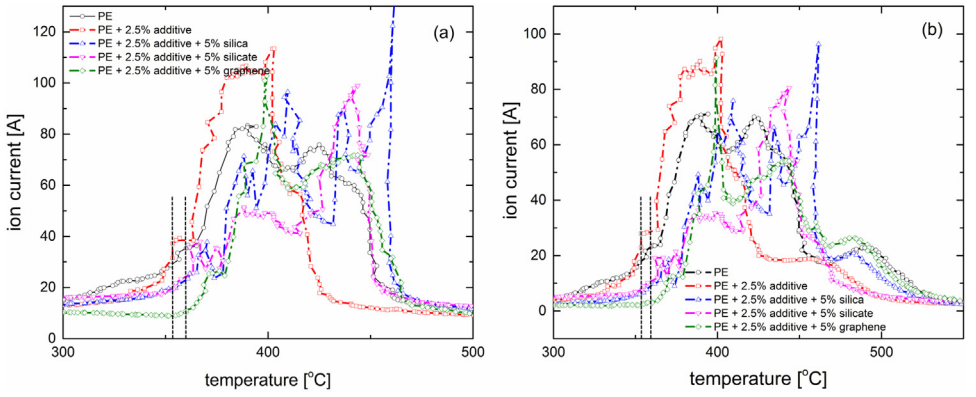


**Fig. 2.** MS spectra of PE, PE-additive blends and PE nanocomposites with 2.5 % additive content, when degraded in air atmosphere (a) for evolution of $H_2O$ (m/z = 18) and (b) for evolution of $CO_2$ (m/z = 44) during thermal degradation.


http://dx.doi.org/10.1016/j.heliyon.2015.e00050

graphene was observed to be most stable with more than 50 °C higher onset of degradation than pure PE. Silica and silicate nanocomposites also exhibited delayed onset of evolution by 20–30 °C for both $H_2O$ and $CO_2$.

Figs. 3a–e show the DSC melting and crystallization thermograms of the additive, PE-additive blends and PE nanocomposites as a function of additive content. The pure additive had a broad melting transition with peak melting and crystallization occurring at 120 °C and 90 °C respectively (Table 2). In comparison, pure PE had peak melting and crystallization temperature of 138 °C and 117 °C respectively. The melt enthalpy in additive was measured to be 102 J/g (normalized to pure polymer) in comparison with 147 J/g for pure PE. Comparing with the melt enthalpy of pure crystalline PE of 293 J/g [30], the extent of crystallinity in the PE and additive were thus 50 % and 35 % respectively. Additive and filler inclusion did not have any appreciable influence on melting or crystallization temperature. In addition, the additive melt transition was not observed in the blends and composites, which indicated that it was mixed well with the matrix polymer. In contrast to melting and crystallization temperatures, significant changes were observed in the melt enthalpy of the polymer with both additive and filler. With 1 % additive content in PE, the melt enthalpy of polymer was increased to 158 J/g, which was further increased to 160 J/g on enhancing the additive content to 2.5 %. This indicated that the additive had the nucleation effect, probably due to the presence of metal particles. However, this effect did not result in any change in the melting and crystallization transitions. Different additive type e.g. metal deactivators have also been reported to have simultaneous nucleation effect even at very low concentrations [31]. Addition of filler further enhanced the melt enthalpy of PE in the composites, which was also enhanced on increasing the additive content. Graphene was observed to cause maximum increment in the melt enthalpy of polymer. For instance, the composite with 5 % graphene and 2.5 % additive content exhibited the melt enthalpy of 169 J/g. Earlier studies have also related the increment of melt enthalpy to the state of filler dispersion in the matrix [32, 33, 34]. It may, thus, indicate that graphene platelets had better dispersion in the composite than the silica and silicate fillers. Large aspect ratio of the graphene platelets could have also contributed to this effect. Thus, the changes in properties of the composites would have resulted from both crystallinity increase as well as filler itself. Fig. 3f also demonstrates the increase in relative crystallinity as a function of additive content. An increment of ~8 % was observed for the graphene composite with 2.5 % additive content.

The miscibility of the PE-additive blends was studied using Cole-Cole viscosity plot by developing relationships between real ($\eta'$) and imaginary ($\eta''$) parts of complex viscosity [35, 36, 37]. As can be seen in Fig. 4a, both blends exhibited semi-circular shape indicating the miscible phase morphology in the blends,


http://dx.doi.org/10.1016/j.heliyon.2015.e00050

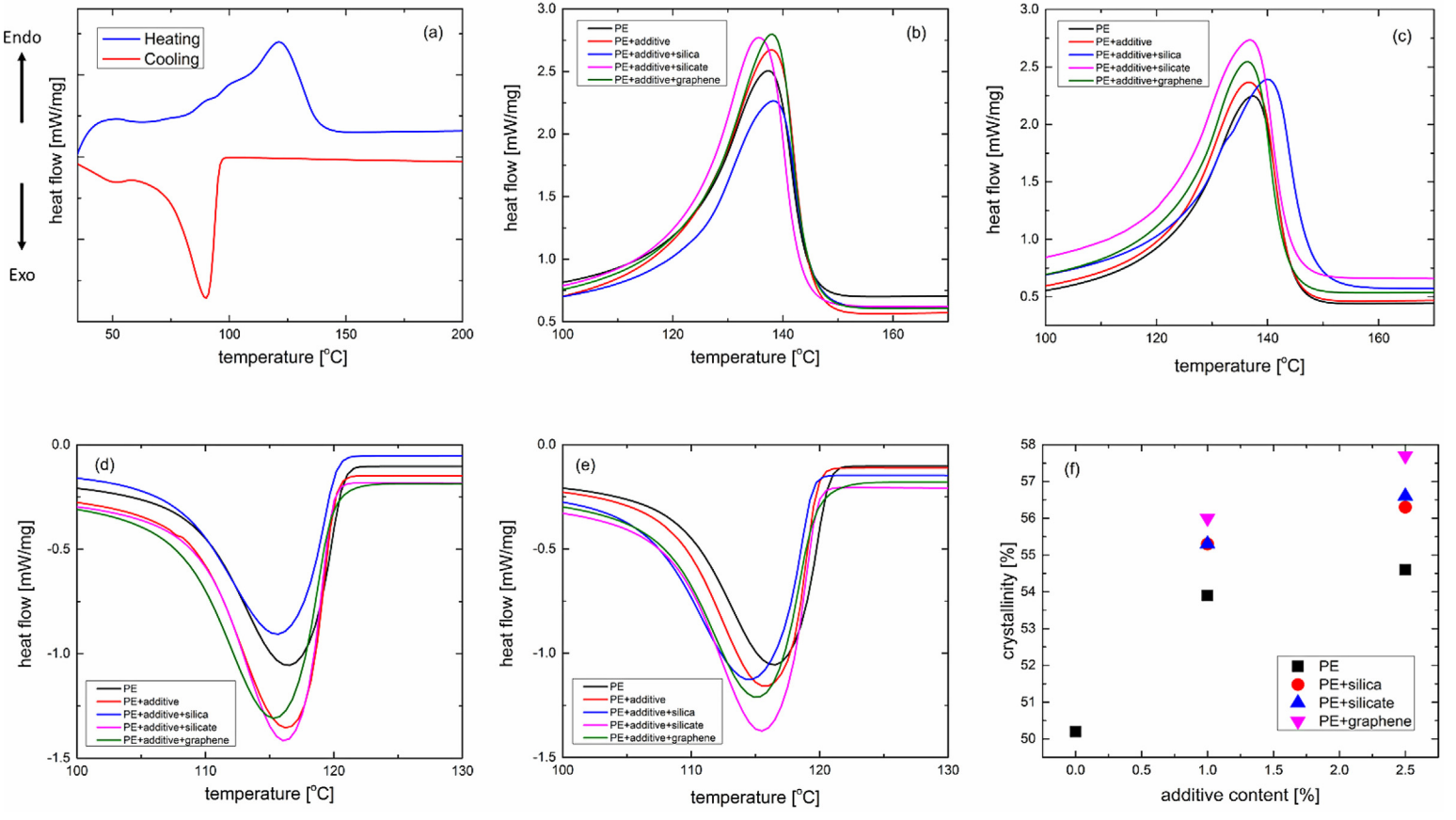


**Fig. 3.** DSC melting thermograms of (a) additive, PE, PE-additive blends and PE nanocomposites for (b) 1 % additive and (c) 2.5 % additive content; (d) and (e) are respective crystallization curves; (f) changes in relative crystallinity for these materials as a function of additive content.





http://dx.doi.org/10.1016/j.heliyon.2015.e00050

**Table 2.** Calorimetric properties of PE, PE-additive blends and PE nanocomposites.

| Polymer/Nanocomposite | Peak melting point, $T_m$ [°C] | Peak crystallization temperature, $T_c$ [°C] | Enthalpy, ΔH [J/g] |
|---|---|---|---|
| Additive | 120 | 90 | 102 |
| Pure PE | 138 | 117 | 147 |
| PE + 1 % additive | 138 | 117 | 158 |
| PE + 2.5 % additive | 137 | 116 | 160 |
| PE + 1 % additive + 5 % silica | 138 | 116 | 160 |
| PE + 2.5 % additive + 5 % silica | 140 | 115 | 161 |
| PE + 1 % additive + 5 % silicate | 136 | 116 | 162 |
| PE + 2.5 % additive + 5 % silicate | 137 | 115 | 166 |
| PE + 1 % additive + 5 % graphene | 138 | 115 | 164 |
| PE + 2.5 % additive + 5 % graphene | 137 | 115 | 169 |

irrespective of the additive content. The observation of phase miscibility also confirmed the DSC findings. Figs. 4b–c show the storage modulus of the PE-additive blends and PE nanocomposites as a function of angular frequency and additive content. The modulus increased for all the samples especially at lower frequency and subsequently exhibited plateau region with lower rate of subsequent increase with angular frequency. The addition of 1 % additive did not change the storage modulus of the polymer. Enhancing the amount of additive further decreased the storage modulus in the lower frequency region probably due to matrix plasticization. Addition of fillers enhanced the modulus significantly due to reinforcement effect. Enhancing the additive content in the composite also enhanced the modulus further indicating that the filler and additive may have synergistic effects on the property enhancement of matrix. Silica and silicate exhibited similar response, whereas graphene had the largest increment in the storage modulus over the whole range of angular frequency. Fig. 4d also demonstrates the comparison of increment in the storage modulus as a function of additive content for 1 rad.$s^{-1}$ and 10 rad.$s^{-1}$ angular frequency. For instance, pure polymer had storage modulus of 41,470 Pa and 48,650 Pa at angular frequency of 1 rad.$s^{-1}$ and 10 rad.$s^{-1}$, which was enhanced to 234,000 Pa and 289,000 Pa respectively in graphene nanocomposite with 2.5 % additive content. The loss modulus showed similar trend as storage modulus and was dependent on filler and additive content. Fig. 4e also shows the complex viscosity profiles as a function of angular frequency. Viscosity followed the similar trends as modulus with graphene composites enhancing the viscosity to maximum extent. However, the viscosity of the composites was still in processable range and the composites did not exhibit any change in processing requirements as compared to pure polymer.


http://dx.doi.org/10.1016/j.heliyon.2015.e00050

http://dx.doi.org/10.1016/j.heliyon.2015.e00050







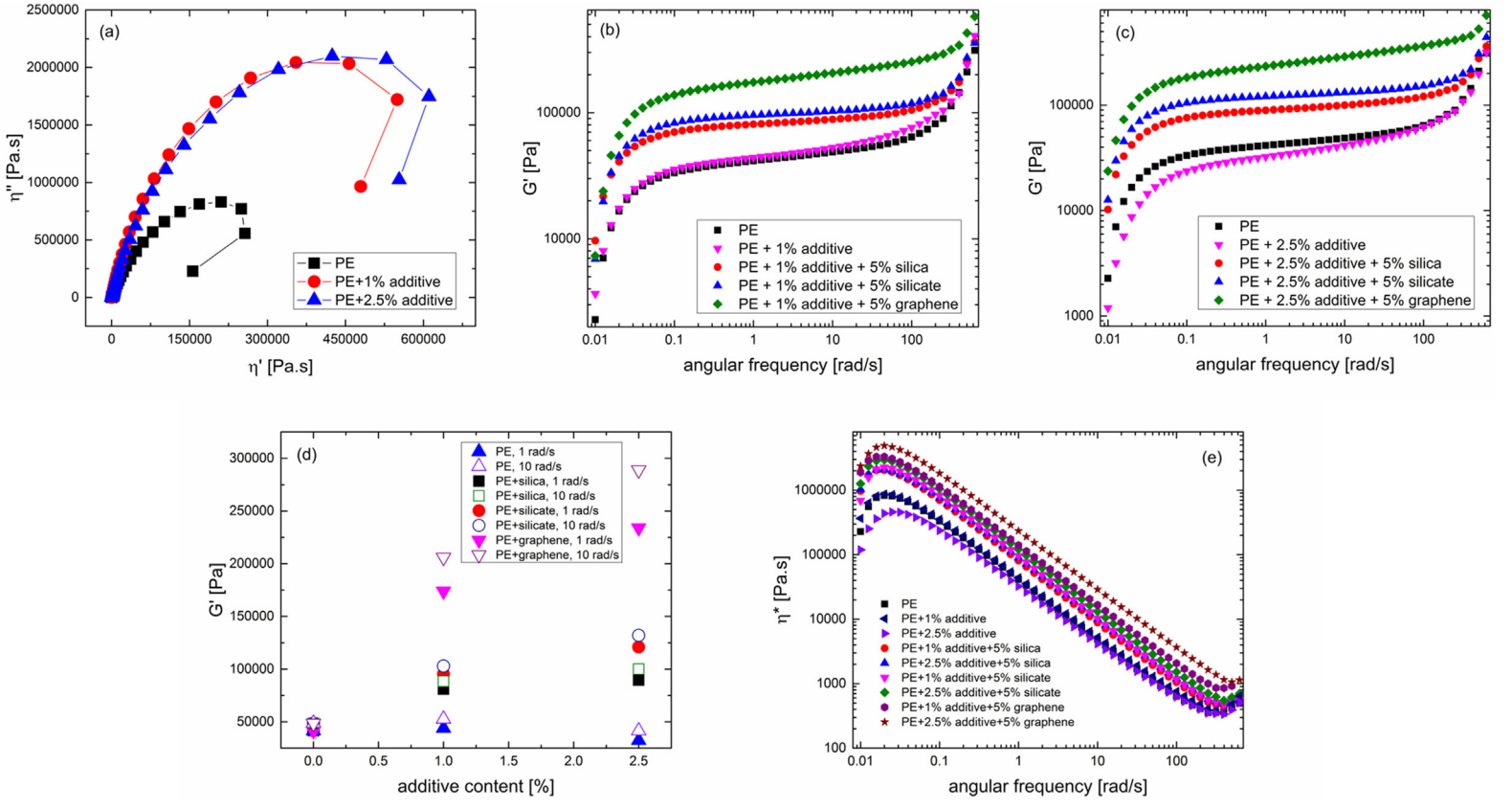


**Fig. 4.** (a) Cole-Cole plots of PE and PE-additive blend samples; storage modulus of PE, PE-additive blends and nanocomposites as a function of angular frequency for (b) 1 % additive and (c) 2.5 % additive content; (d) comparison of storage modulus in the nanocomposites as a function of additive content at an angular frequency of 1 rad.s$^{-1}$ (solid dots) and 10 rad.s$^{-1}$ (empty dots); (e) complex viscosity of the PE, PE-additive blends and PE nanocomposites as a function of angular frequency.

Fig. 5 demonstrates the storage modulus of PE-additive blends and PE nanocomposites as a function of temperature. The modulus curves of PE and PE + 1 % additive blend were observed to overlap with each other at higher temperatures, whereas 2.5 % additive content exhibited reduction in modulus. Moreover, large decrease in the modulus was observed on increasing the temperature from 30 to 100 °C. Silica and silicate nanocomposites exhibited similar behavior beyond 50 °C, whereas graphene nanocomposites had much higher modulus over the whole temperature range indicating superior reinforcing effect. For instance, as compared to pure PE, graphene nanocomposite with 1 % additive content had 40 % and 33 % increment in storage modulus at 50 °C and 70 °C respectively. In comparison to storage modulus, the loss modulus of the PE-additive blends and PE nanocomposites exhibited much lower values, however, the difference between the magnitude of storage and loss moduli reduced with temperature. Except for graphene nanocomposites, loss modulus values of different materials did not vary significantly with filler type or additive content.

Table 3 and Fig. 6a detail the tensile properties of the PE-additive blends and PE nanocomposites. Presence of additive resulted in slight increment in the modulus of PE, though a reduction in tensile strength and enhancement in elongation at break were observed with increasing additive content due to a small extent of matrix plasticization. It should also be noted that the observed effects resulted from combination of factors like increase in crystallinity due to the nucleating effect of the metal particles in the additive as well as matrix plasticization. Addition of fillers resulted in enhancement of tensile modulus, which was further improved on increasing the extent of additive. Fig. 6b also quantifies the increment in modulus of the nanocomposites as a function of additive content. The graphene composite with 2.5 % additive content exhibited nearly 100 % increase in the modulus as compared to pure PE. Similar to

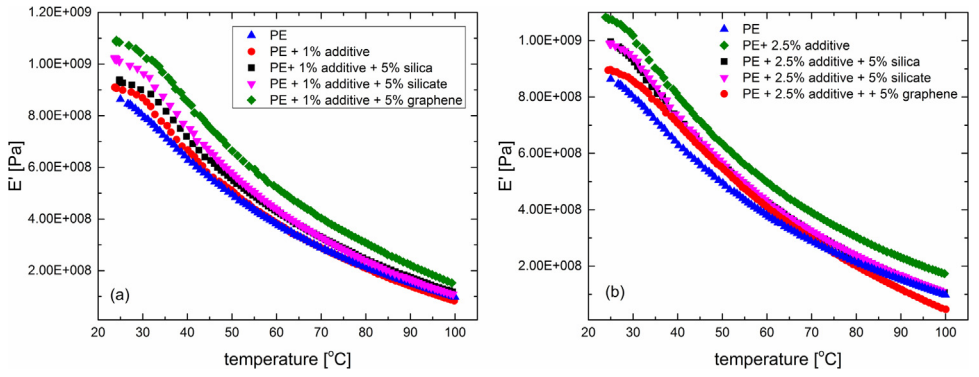


**Fig. 5.** Storage modulus of PE, PE-additive and PE nanocomposites as a function of temperature for (a) 1 % additive and (b) 2.5 % additive content.


http://dx.doi.org/10.1016/j.heliyon.2015.e00050

**Table 3.** Tensile properties of PE, PE-additive blends and PE nanocomposites with 5 % filler content.

| Polymer/Nanocomposite | Young's modulus[a] (MPa) | Tensile strength[b] (MPa) | Elongation at break[c] (mm) |
|---|---|---|---|
| Pure PE | 970 | 24 | 29.5 |
| PE + 1 % additive | 1007 | 23 | 35.0 |
| PE + 2.5 % additive | 1013 | 22 | 37.8 |
| PE + 1 % additive + 5 % silica | 1121 | 23 | 18.0 |
| PE + 2.5 % additive + 5 % silica | 1316 | 23 | 21.6 |
| PE + 1 % additive + 5 % silicate | 1163 | 21 | 15.7 |
| PE + 2.5 % additive + 5 % silicate | 1398 | 21 | 25.0 |
| PE + 1 % additive + 5 % graphene | 1637 | 23 | 0.84 |
| PE + 2.5 % additive + 5 % graphene | 1891 | 21 | 0.90 |

[a] Relative probable error 3 %.
[b] Relative probable error 3 %.
[c] Relative probable error 10 %.

rheological performance, silica composites exhibited least increase in the modulus among the composites. The tensile strength was observed to slightly decrease in the composites due to strain hardening as well as entrapment of polymer chains in the filler interlayers. The elongation at break for graphene nanocomposites was decreased significantly and the composites became brittle (Fig. 6a). In contrast, silica and silicate nanocomposites had still relatively high flexibility, which was enhanced on increasing the additive content in the composite.

X-ray diffractograms in Fig. 7 indicated that main diffraction peaks in the PE were observed at 22.0° and 24.4° 2θ, which corresponded to 110 ad 200 planes. Silica and silicate had characteristic $d_{001}$ diffraction peak at 2θ 20.2° and 24.2°

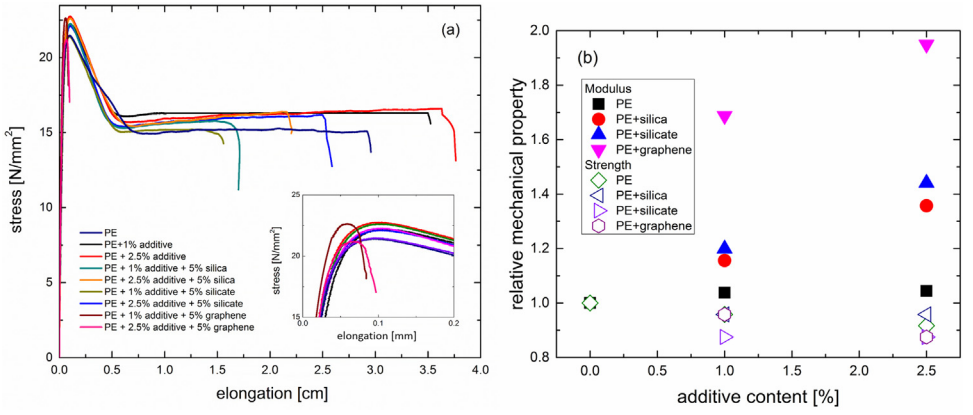


**Fig. 6.** (a) Stress-strain plots of PE, PE-additive blends and nanocomposites. The inset shows the region of yielding and lower elongation of graphene nanocomposites; (b) relative tensile modulus and strength of these materials plotted as a function of additive content.


http://dx.doi.org/10.1016/j.heliyon.2015.e00050

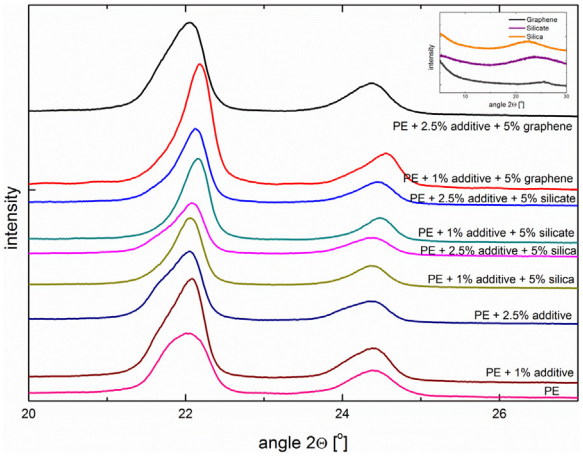


**Fig. 7.** X-ray diffractograms demonstrating the peaks from PE crystalline planes for PE, PE-additive blends and PE nanocomposites. The inset shows the diffraction patterns of the pure fillers.

respectively, whereas thermally reduced graphene exhibited diffraction signal at 25.5°. The addition of additive did not lead to any changes in the diffraction peaks of pure PE, though broadening of the diffraction signals was observed. In the nanocomposites, no filler peaks were observed indicating the shear mixing with polymer resulted in disturbing the ordering between the filler particles (or platelets), thus, intercalating the polymer chains in the interlayers of filler particles. In the composites with 2.5 % additive, the polymer crystalline structure had also minor changes as the diffraction peaks were observed to shift to lower angles, a phenomenon more predominant in graphene and silicate nanocomposites. Efficient filler dispersion in the matrix would have resulted in such changes in polymer diffraction patterns. As mentioned earlier, this would subsequently lead the filler particles to efficiently nucleate the polymer crystallization, as observed earlier in DSC studies. The diffraction signals in graphene and silicate composites were also sharper and more intense due to enhancement of crystallinity, thus further confirming the DSC findings. Fig. 8

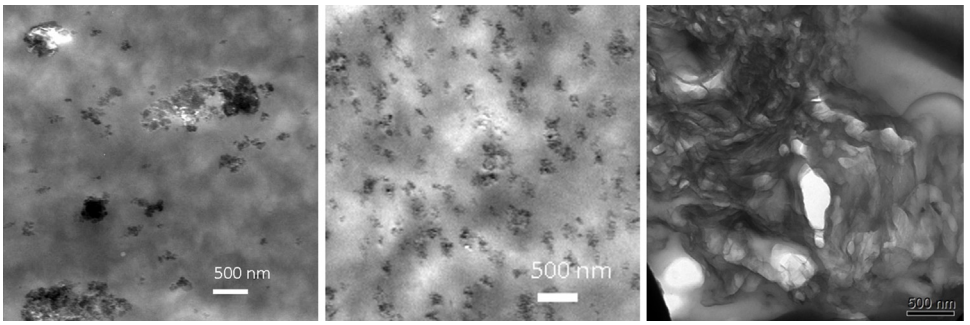


**Fig. 8.** Transmission electron micrographs of PE + 2.5 % additive + 5 % filler nanocomposites: (a) silica, (b) silicate and (c) graphene. The dark lines in Fig. 8(c) represent the cross-section of graphene platelets.


http://dx.doi.org/10.1016/j.heliyon.2015.e00050

shows the TEM micrographs of the composites with 2.5 % additive content. Silicate and graphene composites exhibited uniform nano-scale filler dispersion with no presence of large filler aggregates, thus confirming the observations from X-ray diffraction. Much higher aspect ratio of the graphene platelets was also confirmed, which can be attributed to superior performance of the graphene based nanocomposites. Filler dispersion in silica containing nanocomposites was however less optimum as large aggregates were occasionally present. It, thus, resulted in less significant effect on polymer crystallinity and mechanical properties.

As oxo-degradation causes the formation of a carbonyl group at every scission location in the polymer chains, measurement of the onset and level of carbonyl group development in the specimen is a more accurate measure of induced degradation by the metal ion pro-oxidant. Fig. 9 demonstrates the degree of embrittlement of the samples with 2.5 % additive calculated from the carbonyl index measurements as a function of exposure time adjusted to real environment in a constant temperature of 30 °C in sunlight. PE sample containing only 2.5 % additive exhibited the fastest rate of degradation reaching 100 % embrittlement after ~795 accelerated ageing hours (equivalent to around 8.7 months at 30 °C). The two nanocomposites with 5 % silica and 5 % silicate performed similarly to each other, with the silica containing composite reaching 100 % embrittlement after ~1443 accelerated ageing hours (equivalent to around 15.8 months at 30 °C) and the silicate composite after ~1279 accelerated ageing hours (equivalent to around 15 months at 30 °C). The graphene based composite did not reach 100 % embrittlement during the test period, but was still ~ 48.2 % embrittled at the end of the test. Images in Fig. 10 also show the visual embrittlement of these materials before and after photo-oxidation. The literature studies [21, 22]

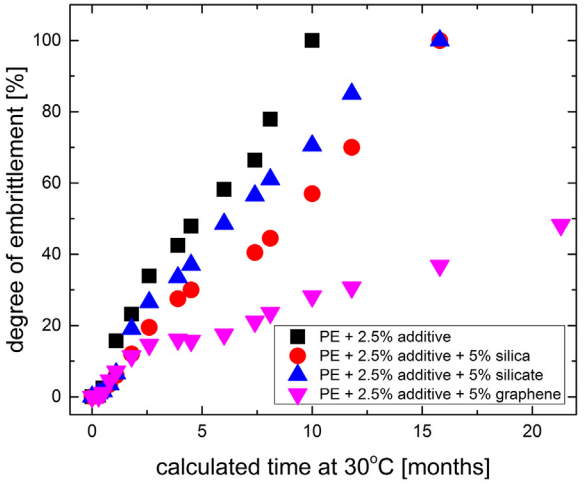


**Fig. 9.** Degree of embrittlement of the materials during photo-degradation testing plotted as a function of time of exposure.


http://dx.doi.org/10.1016/j.heliyon.2015.e00050

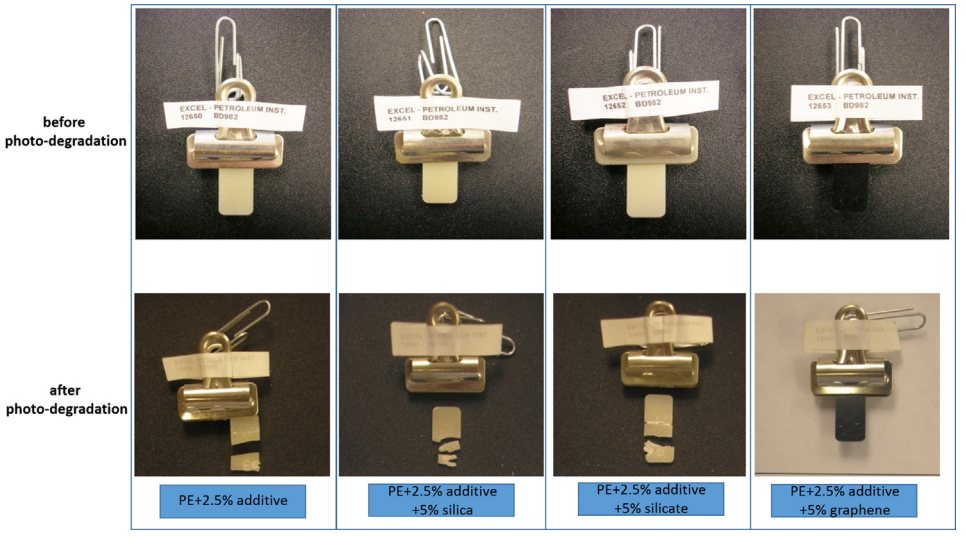


**Fig. 10.** Images of the samples (a) before and (b) after the photo-degradation testing. First image corresponds to PE + 2.5 % additive, whereas second, third and fourth images represent PE + 2.5 % additive + 5 % filler nanocomposites with silica, silicate and graphene respectively.

reported that the organically modified silicate acted both as filler and pro-oxidant. However, the pro-oxidant role was attributed to the presence of ammonium ion in the organic modification, without which the UV degradation may not occur. Kumanakaya [24] also reported that hindrance to oxygen permeation in the matrix in composites reduced the photo-oxidation behavior. Thus, in the current study, the observed decrease in the photo-oxidation of polymer due to the addition of fillers resulted from combination of two factors: increase in extent of photo-oxidation by the addition of pro-oxidant and decrease in the phenomenon by the filler particles due to decrease in oxygen permeation in the matrix. Furthermore, graphene platelets slowed the photo-oxidation to the largest extent due to known property of strong UV absorption by the graphene platelets. However, the observed results confirmed that the addition of pro-oxidant in the composites was necessary to attain their degradation and a controlled and fairly fast degradation could still be achieved even in thick composite plaques with 5 % filler content, especially in silica and silicate containing composites. These results thus demonstrated the successful generation of nanocomposites with oxo-biodegradable additive which had much superior mechanical, thermal and rheological properties and had additional functionality of photo-oxidation, subsequently leading to their bio-degradation.

## 4. Conclusions

Polyethylene nanocomposites containing different fillers and varying amount of oxo-biodegradation additive were generated by melt mixing. The additive was observed to be miscible with PE at both 1 % and 2.5 % concentration.


http://dx.doi.org/10.1016/j.heliyon.2015.e00050

Incorporation of additive led to reduction in thermal stability of PE without changing the degradation mechanism of polymer, whereas fillers delayed the onset and peak degradation temperatures. Graphene exhibited highest impact on thermal stability as the peak degradation temperature was increased by 13–14 °C in the composites as compared to pure PE. Both additive and fillers did not affect the peak melting and crystallization temperature of PE, however, the enthalpy was observed to increase indicating their nucleating effect on the polymer. Due to higher aspect ratio and efficient filler dispersion, graphene based nanocomposites were observed to have maximum enhancement in polymer crystallinity. Graphene nanocomposites had highest extent of increment in storage modulus which was further enhanced as the additive content was increased. Similarly, tensile modulus of graphene nanocomposites was 1.70 times than pure PE for 5 % filler content and 1 % additive concentration. Silicate and silica based composites exhibited increments of 1.20 and 1.16 times thus indicting lower extent of polymer reinforcement. The additive did not show antagonistic effect on filler or composite performance and increasing the additive content to 2.5 % led to enhancements of modulus to 1.95, 1.44 and 1.36 times respectively for graphene, silicate and silica composites. Viscosity of the composites remained still processable similarly as pure PE. The crystalline structure in graphene and silicate nanocomposites had also minor changes as the diffraction peaks were observed to shift to lower angles. The morphology of these composites was more delaminated as compared to silica composites, where occasionally large filler aggregates were present. Complete photo-oxidation of the thick plaques of silica and silicate composites with 2.5 % additive could be successfully achieved to be 15–16 months at 30 °C, though it was slowed down as compared to 9 months for polymer-additive blend. In addition, graphene composite was also photo-degraded to nearly 50 % in the same time period, even in the presence of large aspect ratio graphene platelets. These results indicated that the additive contributed efficiently to the crystallinity and mechanical performance of the nanocomposites and resulted in fairly fast degradation even for thick specimens.

## Declarations

## Author contribution statement

Fakhruddin Patwary: Performed the experiments; Analyzed and interpreted the data.

Vikas Mittal: Conceived and designed the experiments; Analyzed and interpreted the data; Contributed reagents, materials, analysis tools or data; Wrote the paper.


http://dx.doi.org/10.1016/j.heliyon.2015.e00050

## Funding statement

This work was supported by The Petroleum Institute Research Initiation Funding Program (Project 13,309).

## Competing interest statement

The authors declare no conflict of interest.

## Additional information

No additional information is available for this paper.

## Acknowledgements

Extensive support of Wells Plastics in studying the photo-degradation performance of materials at their facility in Staffordshire, UK is highly appreciated.

## References

[1] R. Smith (Ed.), Biodegradable polymers for industrial applications, Woodhead Publishing Limited, England, 2005.

[2] A.A. Shah, F. Hasan, A. Hameed, S. Ahmed, Biological degradation of plastics: A comprehensive review, Biotechnol. Adv. 26 (3) (2008) 246–265.

[3] A.C. Albertsson, S.O. Andersson, S. Karlsson, The mechanism of biodegradation of polyethylene, Polym. Degrad. Stabil. 18 (1) (1987) 73–87.

[4] B. Erlandsson, S. Karlsson, A.C. Albertsson, The mode of action of corn starch and a pro-oxidant system in LDPE: influence of thermo-oxidation and UV-irradiation on the molecular weight changes, Polym. Degrad. Stabil. 55 (2) (1997) 237–245.

[5] H.S. Hamid, M.B. Amin, A.G. Maadhah, Handbook of polymer degradation, Marcel Dekker Inc, New York, 1992.

[6] A.C. Albertsson, S. Karlsson, Degradable polymers for the future, Acta Polym. 46 (2) (1995) 114–123.

[7] P.K. Roy, P. Surekha, C. Rajagopal, V. Choudhary, Effect of cobalt carboxylates on the photo-oxidative degradation of low-density polyethylene Part-I, Polym. Degrad. Stabil. 91 (9) (2006) 1980–1988.

 http://dx.doi.org/10.1016/j.heliyon.2015.e00050

[8] N. Sharma, L.P. Chang, Y.L. Chu, H. Ismail, U.S. Ishiaku, M. Ishak, A study on the effect of pro-oxidant on the thermo-oxidative degradation behaviour of sago starch filled polyethylene, Polym. Degrad. Stabil. 71 (3) (2001) 381–393.

[9] N.B. Vogt, E.A. Kleppe, Oxo-biodegradable polyolefins show continued and increased thermal oxidative degradation after exposure to light, Polym. Degrad. Stabil. 94 (4) (2009) 659–663.

[10] I. Jakubowicz, Evaluation of degradability of biodegradable polyethylene (PE), Polym. Degrad. Stabil. 80 (1) (2003) 39–43.

[11] J.K. Pandey, R.P. Singh, UV-irradiated biodegradability of ethylene-propylene copolymers, LDPE and iPP in composting and culture environments, Biomacromolecules 2 (3) (2001) 880–885.

[12] T. Lan, P.D. Kaviratna, T.J. Pinnavaia, On the nature of polyimidie-clay hybrid composites, Chem. Mater. 6 (1994) 573–575.

[13] I.-J. Chin, T. Thurn-Albrecht, H.-C. Kim, T.P. Russell, J. Wang, On exfoliation of montmorillonite in epoxy, Polymer 42 (2001) 5947–5952.

[14] S.K. Lim, J.W. Kim, I.-J. Chin, Y.K. Kwon, H.J. Choi, Preparation and interaction characteristics of organically modified montmorillonite nanocomposite with miscible polymer blend of poly(ethylene oxide) and poly(methyl methacrylate), Chem. Mater. 14 (2002) 1989–1994.

[15] Z. Wang, T.J. Pinnavaia, Nanolayer reinforcement of elastomeric polyurethane, Chem. Mater. 10 (1998) 3769–3771.

[16] P.B. Messersmith, E.P. Giannelis, Synthesis and barrier properties of poly(tdtmp:straightepsilon-caprolactone)-layered silicate nanocomposites, J. Polym. Sci. A Polym. Chem. 33 (1995) 1047–1057.

[17] K. Yano, A. Usuki, A. Okada, Synthesis and properties of polyimide-clay hybrid films, J. Polym. Sci. A Polym. Chem. 35 (1997) 2289–2294.

[18] H. Shi, T. Lan, T.J. Pinnavaia, Interfacial effects on the reinforcement properties of polymer/organoclay nanocomposites, Chem. Mater. 8 (1996) 1584–1587.

[19] E.P. Giannelis, Polymer layered silicate nanocomposites, Adv. Mater. 8 (1996) 29–35.

[20] P.C. LeBaron, Z. Wang, T.J. Pinnavaia, Polymer layered silicate nanocomposites: an overview, Appl. Clay Sci. 15 (1999) 11–29.

 http://dx.doi.org/10.1016/j.heliyon.2015.e00050

[21] A. Tidjani, C.A. Wilkie, Photo-oxidation of polymeric-inorganic nanocomposites: chemical, thermal stability and fire retardancy investigations, Polym. Degrad. Stabil. 74 (1) (2001) 33–37.

[22] H. Qin, C. Zhao, S. Zhang, G. Chen, M. Yan, Photo-oxidative degradation of polyethylene/montmorillonite nanocomposite, Polym. Degrad. Stabil. 81 (3) (2003) 497–500.

[23] C. Espejo, A. Arribas, F. Monzo, P.P. Diez, Nanocomposite films with enhanced radiometric properties for greenhouse covering applications, J. Plast. Film Sheeting 28 (4) (2012) 336–350.

[24] T.O. Kumanayaka, Photo-oxidation and biodegradation of polyethylene nanocomposites, PhD Thesis, RMIT University, Australia, 2010.

[25] Wells Plastics, Oxo-biodegradable additive masterbatches (online), Available from: http://www.wellsplastics.com/httdocs/resources/Wells_Reverte_Brochure.pdf (2014) (Accessed: 25.04.14).

[26] A.U. Chaudhry, V. Mittal, High-density polyethylene nanocomposites using masterbatches of chlorinated polyethylene/grapheme oxide, Polym. Eng. Sci. 53 (1) (2013) 78–88.

[27] M.J. McAllister, J.L. Li, D.H. Adamson, H.C. Schniepp, A.A. Abdala, J. Liu, M. Herrera-Alonso, D.L. Milius, R. Car, R.K. Prud'homme, I.A. Aksay, Single sheet functionalized graphene by oxidation and thermal expansion of graphite, Chem. Mater. 19 (2007) 4396–4404.

[28] J.H. Lee, D. Jung, C.E. Hong, K.Y. Rhee, S.G. Advani, Properties of polyethylene-layered silicate nanocomposites prepared by melt intercalation with a PP-g-MA compatibilizer, Compos. Sci. Technol. 65 (2005) 1996–2002.

[29] P. Reichert, H. Nitz, S. Klinke, R. Brandsch, R. Thomann, R. Mulhaupt, Poly(propylene)/organoclay nanocomposite formation: influence of compatibilizer functionality and organoclay modification, Macromol. Mater. Eng. 275 (2000) 8–17.

[30] M. Joshi, B.S. Butola, G. Simon, N. Kukaleva, Rheological and viscoelastic behavior of HDPE/octamethyl-POSS nanocomposites, Macromolecules 39 (2006) 1839–1849.

[31] T. Yoshikawa, K. Kimura, Effect of crystal nucleation by copper deactivator on aging life of polypropylene, Materials Life 10 (3) (1998) 143–148.

 http://dx.doi.org/10.1016/j.heliyon.2015.e00050

[32] W. Xu, G. Liang, H. Zhai, S. Tang, G. Hang, W.P. Pan, Preparation and crystallization behavior of PP/PP-g-MAH/org-MMT nanocomposite, Eur. Polym. J. 39 (2003) 1467–1474.

[33] P. Maiti, P.H. Nam, M. Okamoto, T. Kotaka, N. Hasegawa, A. Usuki, The effect of crystallization on the structure and morphology of polypropylene/clay nanocomposites, Polym. Eng. Sci. 42 (2002) 1864–1871.

[34] J. Ma, S. Zhang, Z. Qi, G. Li, Y. Hu, Crystallization behaviors of polypropylene/montmorillonite nanocomposites, J. Appl. Polym. Sci. 83 (2002) 1978–1985.

[35] K. Cho, B.H. Lee, K.M. Hwang, H. Lee, S. Choe, Rheological and mechanical properties in polyethylene blends, Polym. Eng. Sci. 38 (1998) 1969–1975.

[36] H.K. Kim, D. Rana, H. Kwag, S. Choe, Melt rheology of ethylene 1-octene copolymer blends synthesized by Ziegler-Natta and metallocene catalysts, Korea Polym. J. 8 (2001) 34–43.

[37] H. Kwag, D. Rana, K. Cho, J. Rhee, T. Woo, B.H. Lee, S. Choe, Binary blends of metallocene polyethylene with conventional polyolefins: rheological and morphological properties, Polym. Eng. Sci. 40 (2000) 1672–1681.